Risk-based optimal power flow with probabilistic guarantees

Risk-Based Optimal Power Flow with Probabilistic Guarantees

Line Roald[1*], Maria Vrakopoulou[2], Frauke Oldewurtel[3], Göran Andersson[1]
[1]Power Systems Laboratory, Department of Electrical Engineering, ETH Zurich, Switzerland
[2]Department of Electrical Engineering and Computer Science, University of Michigan, USA
[3]Department of Electrical Engineering and Computer Science, UC Berkeley, USA
*Corresponding Author. E-mail address: roald@eeh.ee.ethz.ch; Tel: +41 44 632 65 77.

***Abstract*—Higher penetration of renewable energy sources and market liberalization increase both the need for transmission capacity and the uncertainty in power system operation. New methods for power system operational planning are needed to allow for efficient use of the grid, while maintaining security against disturbances. In this paper, we propose a risk model for risks related to outages, accounting for available remedial measures and the impact of cascading events. The new risk model is used to formulate risk-based constraints for the post-contingency line flows, which are included in an optimal power flow (OPF) formulation. Forecast uncertainty is accounted for by formulating the relevant constraints as a joint chance constraint, and the problem is solved using a sampling-based technique. In a case study of the IEEE 30 bus system, we demonstrate how the proposed risk-based, probabilistic OPF allows us to control the risk level, even in presence of uncertainty. We investigate the trade-off between generation cost and risk level in the system, and show how accounting for uncertainty leads to a more expensive, but more secure dispatch.**

***Keywords*—risk-based optimal power flow, chance constrained optimal power flow, security, wind power integration**

I. Introduction

Market liberalization and increasing penetration of renewable energy sources (RES) lead to a situation where power is not necessarily produced close to where it is consumed, but rather where production is cheap, the wind is blowing or the sun is shining. This trend increases the need for transmission capacity, and forces the transmission system operators to operate the system closer to the operational limits. At the same time, fluctuations in RES in-feed and short-term trading lead to larger deviations from the planned schedule, and thus increase uncertainty in power system operation. The combination of a highly loaded system and significant uncertainty increases operational risk. There is a need for methods which allow for efficient use of transmission capacity, while maintaining security and robustness against disturbances.

There are two types of disturbances in the system, *random outages* and *forecast uncertainty*, which have inherently different characteristics. Whereas outages can be characterized as discrete events with a (usually) low probability, forecast uncertainty (deviations in power in-feeds arising from load, RES or short-term trading) is characterized by a continuous probability distribution. The method proposed in this paper addresses both types of disturbances. The random outages are handled by a risk-based extension to the N-1 criterion that utilizes additional information about the probability of outages, the extent of post-contingency violations and the cost and availability of remedial actions to provide a more quantitative measure of power system security. The risk-based criterion is implemented in an optimal power flow (OPF). By formulating the OPF as a chance constrained optimization problem, we are able to account for forecast deviations in a comprehensive way. The resulting formulation allows us to control the risk of outages, even in presence of forecast uncertainty.

There exist two main approaches to model risk in power system operation. On the one hand, risk can be modeled through overall reliability parameters like Expected Energy Not Served (EENS). These parameters incorporate the effect of cascading events and thus reflect the risk faced by the customers in the system. However, computing the risk requires extensive calculations (i.e., Monte-Carlo simulations), and these types of risk measures are therefore typically used to analyze the risk for a given operating condition [1], [2], as opposed to inclusion in an optimization problem.

On the other hand, risk can be modeled in terms of violation of technical limits, e.g., dependent on the power flow of a line or on the voltage magnitude. Such risk measures typically consider the situation after an N-1 outage, and do not simulate how a potential cascade would develop further. Thus, these risk measures do not reflect the full risk of cascading events, but are much easier to compute than the risk measures in the first category. Further, when a risk measure is related to specific technical parameters, it is easier for the system operator to identify actions to influence the risk. This type of risk measures have therefore often been proposed for incorporation in OPF formulations. The OPF formulations in [3], [4] describe risk as violations and near-violations of voltage limits and line transfer capacities, modeled as linear functions of the voltage magnitude and the line flow. In [5], risk is expressed as a quadratic function of the line flow, whereas [6] models risk as the cost of equipment aging in function of, e.g., the line flow. Here, risk is expressed as a piecewise affine function of the line flow, based on the risk function we presented in [7]. The parameters of the risk function are computed based on the cost and availability of remedial measures, and also reflects the risk of initiating a cascading event.

The OPF is formulated as a central dispatch problem minimizing overall generation cost, similar to the OPF problems solved in markets with locational marginal pricing (LMP). Recently, [8] investigated how a risk-based OPF impacts the LMPs, showing that the risk-based OPF introduces a new cost component which reflects the system risk level. While [8] also uses a piecewise affine risk function, the parameters of the risk function seem to be chosen arbitrarily, thus impacting

the LMPs in an arbitrary way. In contrast, the parameters introduced in this paper are based on actual system properties, providing a less arbitrary definition of the risk function.

Although the OPF is formulated as a central dispatch problem, the proposed method does not focus on the market clearing aspect, but rather on ensuring that the dispatch has a sufficiently low level of risk. Therefore, it can also be applied in self-dispatch markets by changing the objective to minimize changes to the market outcome instead of minimizing overall generation cost. For security considerations, the relation between the risk function and the cost and availability of remedial measures is particularly interesting. All risk-based formulations [3] - [8] allow for post-contingency line overloading under some circumstances, but do not provide remedial actions to bring the system back to normal operation. Since the risk function proposed here is based on the cost and availability of remedial actions, the method proposes effective post-contingency remedial actions, ensuring that system security can be restored when a contingency occurs.

Although several risk-based OPF formulations exist, few of them account for forecast uncertainty in a comprehensive way. The OPF formulation in [6] considers normally distributed load uncertainty, but only limits the expected value of the risk and does not provide any guarantees for an upper bound. In contrast, the method proposed in this paper guarantees that the risk limit will hold with a chosen probability. This is achieved by formulating a chance constrained optimization problem, following along the lines of [9], [10]. The problem is solved using the randomized optimization technique proposed in [11], based on the so-called scenario approach from [12]. This technique requires no assumptions on the distribution of the forecast errors.

In summary, the contributions of this paper are threefold: 1) We define a risk function based on system parameters such as available remedial measures, which has several advantages compared to previous risk functions. First, it avoids using arbitrary parameters with arbitrary influence on cost. Second, the severity function is defined separately for each line and each contingency. Third, it suggests effective remedial measures for the cases where a post-contingency overload is accepted. 2) We introduce risk-based constraints for post-contingency line flows, and show how to choose appropriate upper bounds on the risk by comparing the risk-based constraints to the deterministic N-1 constraints. 3) We include the risk-based constraints in a chance constrained OPF formulation to account for forecast uncertainty from RES.

The reminder of the paper is organized as follows: Section II introduces the risk measure which relates post-contingency line loading to the cost of remedial measures and the probability of cascading events. Section III formulates a DC optimal power flow incorporating the risk measure and chance constraints to account for forecast uncertainty. Section IV analyzes the proposed formulation and compares it with other OPF formulations with regards to cost, risk level, and number of post-contingency overloads in a case study for the IEEE 30-bus system. An additional sensitivity study investigates the relationship between remedial actions and accepted post-contingency overloads, as well as the proposed remedial actions. Section V summarizes and concludes. Note that this paper is an extension to [7], introducing an improved severity function, additional results and a prolonged discussion.

II. Risk Modeling

In this paper, we propose a risk measure for incorporation in an OPF formulation and focus on risk as a function of post-contingency transmission line loading. Previous risk formulations (e.g., [4], [5]) use the same severity function for all transmission lines independent of which contingency has taken place. Here, we improve this formulation in two ways. First, we explicitly account for different types of risk (such as moderate overloads that can be mitigated through redispatch and high overloads that might lead to cascading events) by formulating a piecewise linear severity function. Second, we formulate the severity function separately for each line and contingency, which allows us to account for the effect of available remedial measures on each line in each post-contingency situation. The proposed risk formulation allow us to set post-contingency line flow limits based on the available remedial measures and potential impacts of cascading events. This ensures that effective remedial measures are available in the cases where we allow for post-contingency overloads.

A. Definition of the risk measures

A risk measure should reflect both the probability of an outage and the severity of the resulting operating condition. The risk related to a specific outage *i* and line *k* is expressed as

$$\boldsymbol{\mathcal{R}}^{spec}_{(i,k)} := \boldsymbol{\mathcal{P}}_{(i)} \cdot \boldsymbol{\mathcal{S}}_{(k|i)} \ , \tag{1}$$

where $\boldsymbol{\mathcal{P}}_{(i)}$ is the probability of outage i and $\boldsymbol{\mathcal{S}}_{(k|i)}$ is the severity of the operating condition on line k given outage i. This expression can be seen as the risk-based counterpart of the N-1 criterion, as it describes the risk for a specific line in one specific post-contingency state. Using $\boldsymbol{\mathcal{R}}^{spec}_{(i,k)}$ as a basis, we define:

$$\boldsymbol{\mathcal{R}}^{out}_{(i)} := \sum_{k=1}^{N_l} \boldsymbol{\mathcal{P}}_{(i)} \cdot \boldsymbol{\mathcal{S}}_{(k|i)} \tag{2}$$

$$\boldsymbol{\mathcal{R}}^{line}_{(k)} := \sum_{i=1}^{N_{out}} \boldsymbol{\mathcal{P}}_{(i)} \cdot \boldsymbol{\mathcal{S}}_{(k|i)} \tag{3}$$

$$\boldsymbol{\mathcal{R}}^{tot} := \sum_{i=1}^{N_{out}} \sum_{k=1}^{N_l} \boldsymbol{\mathcal{P}}_{(i)} \cdot \boldsymbol{\mathcal{S}}_{(k|i)} \tag{4}$$

$\boldsymbol{\mathcal{R}}^{out}_{(i)}$ expresses the risk after an outage i, and is obtained by summing the risk of all lines k in this post-contingency state. $\boldsymbol{\mathcal{R}}^{line}_{(k)}$ is the risk related to line k, summed over all outages i. $\boldsymbol{\mathcal{R}}^{tot}$ is the total risk in the system, summed over all outages i and all lines k.

In order to evaluate (1), the outage probabilities $\boldsymbol{\mathcal{P}}_{(i)}$ must be estimated, and the severity $\boldsymbol{\mathcal{S}}_{(k|i)}$ has to be defined. We assume that the outage probabilities are calculated a-priori (e.g., based on historical data and current weather conditions [13], [14]) and given as an input to the optimization. The severity modeling is described in the next section.

B. Severity modeling

To capture different types of risk arising from different levels of post-contingency line loading, we define the severity $\boldsymbol{\mathcal{S}}_{(k|i)}$ as a piecewise linear function of the line flow. We define four different segments for the severity function (as opposed

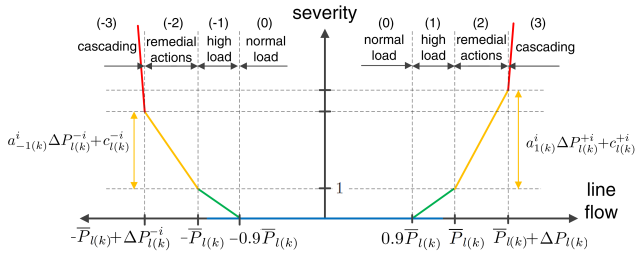

Fig. 1. Piecewise linear severity function for line k after outage i.

to two in previous formulations [4], [5]). The four segments are shown in Fig. 1, and correspond to 0) normal load, 1) high load, 2) moderate overload which requires remedial actions and 3) cascading overload which might lead to a cascading event. For the derivation of the severity function parameters, we consider a system with N_l lines and N_G generators and include the outage of any line or generator, in total $N_{out} = N_l + N_G$ outages. Although we restrict ourselves to those N-1 outages, any other outage situations, e.g. N-2 or common mode outages, can be included without any change to the methodology. The post-contingency line flows after outage i are denoted by the vector $P_l^i \in \mathbb{R}^{N_l}$, with $P_{l(k)}^i$ being the post-contingency flow on the k^{th} line. $\overline{P}_l \in \mathbb{R}^{N_l}$ denote the line capacity limit during normal operation. Mathematically, we define the piecewise linear severity function as the pointwise maximum over a set of affine functions of the line flow,

$$\boldsymbol{\mathcal{S}}_{(k|i)}(P_{l(k)}^i) := \max_j \{a_{j(k)}^i P_{l(k)}^i + b_{j(k)}^i\} \ , \ j \in \{-3, ..., 3\} \tag{5}$$

where $a_{j(k)}^i, b_{j(k)}^i$ are parameters for the j^{th} segment belonging to line k and outage i. Formulating the severity function like this ensures tractability of the optimization problem, as discussed in Section III.A. We will now give a physical interpretation of the different severity zones, and explain how to compute the parameters $a_{j(k)}^i$ and $b_{j(k)}^i$ with $j = 0, ..., 3$ for positive line flows. The severity function is not symmetric in general, but the parameters for negative line flows with $j = -3, ..., 0$ can be calculated in an analogue way.

1) Normal load: At low load ($P_{l(k)}^i < 0.9 \cdot \overline{P}_{l(k)}$), the severity is assumed to be zero. This segment of the severity function, marked blue in Fig. 1, connects the two points

$$\boldsymbol{\mathcal{S}}_{(k|i)}(0) = 0 \tag{6}$$

$$\boldsymbol{\mathcal{S}}_{(k|i)}(0.9 \cdot \overline{P}_{l(k)}) = 0 \ , \tag{7}$$

with parameters $a_{0(k)}^i = b_{0(k)}^i = 0$.

2) High load: High loading ($0.9 \cdot \overline{P}_{l(k)} < P_{l(k)}^i < \overline{P}_{l(k)}$) might lead to a failure of the line (e.g., due to relay malfunction), and the severity is therefore non-zero. We choose $a_{1(k)}^i$ and $b_{1(k)}^i$ such that the "high load" segment of the severity function connects the two points given by Eq. (7) and (8). This segment is marked green in Fig. 1.

$$\boldsymbol{\mathcal{S}}_{(k|i)}(\overline{P}_{l(k)}) = 1 \ . \tag{8}$$

3) Moderate overload: Many system operators allow a transmission line overload for a short time (e.g., for a short period after a contingency). However, if the operating limit is violated, removing the overload requires remedial actions like transmission switching or redispatch. Here, we define moderate overload as one which can be relieved within a given time frame (e.g., 5 minutes). The corresponding severity zone goes from $\overline{P}_{l(k)} < P_{l(k)}^i < (\overline{P}_{l(k)} + \Delta P_{l(k)}^{+i})$, where we define $\Delta P_{l(k)}^{+i}$ as the largest achievable line flow reduction for line k after outage i. $\Delta P_{l(k)}^{+i}$ is a function of the available remedial measures (e.g., available redispatch). The effectiveness of a remedial measure depends on the location of a line in the system, topology changes (e.g., after a line outage), or changes in availability of remedial measures (e.g., after the outage of a generator offering redispatch). Therefore, $\Delta P_{l(k)}^{+i}$ must be calculated separately for each line and each outage. The increase in risk from $\overline{P}_{l(k)}$ to $(\overline{P}_{l(k)} + \Delta P_{l(k)}^{+i})$ depends on both the risk of overloading the line and the cost of removing this overload. The cost of reducing the line flow by $\Delta P_{l(k)}^{+i}$ is denoted by $c_{l(k)}^{+i}$, and can be a function of, e.g., the cost of a redispatch measure. Some remedial measures, such as switching measures, does not incur any additional cost ($c_{l(k)}^{+i} = 0$). However, allowing for a temporary overload always involves an increase in the risk since the probability of an outage increases (due to increased line sag and higher probability of relay malfunction) and the remedial actions might not work as planned. This inherent risk of overloading is therefore modelled in a similar way as for the high load case, with the same slope $a_{1,k}^i$. If both $\Delta P_{l(k)}^{+i}$ and $c_{l(k)}^{+i}$ are known, the severity function parameters $a_{2(k)}^i$ and $b_{2(k)}^i$ are chosen such that the severity function connects the two points given by (8) and (9). This segment is marked yellow in Fig. 1.

$$\boldsymbol{\mathcal{S}}_{(k|i)}(\overline{P}_{l(k)} + \Delta P_{l(k)}^{+i}) = 1 + a_{1(k)}^i \Delta P_{l(k)}^{+i} + c_{l(k)}^{+i} \ . \tag{9}$$

The term $a_{1(k)}^i \Delta P_{l(k)}^{+i}$ represent the inherent risk of overloading, and $c_{l(k)}^{+i}$ the cost of the remedial action. Note that the severity function (5) is convex for all remedial actions, since $a_{2(k)}^i \geq a_{1(k)}^i$.

In general, there are many ways to consider remedial measures in this formulation. We now suggest one way of defining $\Delta P_{l(k)}^{+i}$ and $c_{l(k)}^{+i}$ with the following choice: (i) We only consider generation redispatch. (ii) We only allow one redispatch measure (i.e., one shift between two generators) per line and contingency. We further assume that the available positive and negative redispatch is known and given by the vectors $P_R^+, P_R^- \in \mathbb{R}_{+0}^{N_G}$, with $P_{R(g)}^+$ denoting the positive redispatch capability of generator g. The corresponding redispatch costs are also assumed to be known and are given by $c_R^+, c_R^- \in \mathbb{R}^{N_G}$. To compute the largest possible reduction of the line flow $\Delta P_{l(k)}^{+i}$, we first need to compute the largest possible shift in generation $\Delta P_{g \to h}$ from any generator g to any other generator h. This is given by

$$\Delta P_{g \to h} = \min\{P_{R(g)}^+, P_{R(h)}^-\} \ . \tag{10}$$

To describe how much a generation shift from g to h decreases the power flow on line k, we use the power transfer distribution factor $PTDF_{k,g \to h}$ [15]. The largest power flow decrease $\Delta P_{l(k)}^{i+}$ can then be calculated as

$$\Delta P_{l(k)}^{+i} = -\min_{g,h}\{PTDF_{k,g \to h}^i \Delta P_{g \to h}^i\} \ , \tag{11}$$

since $\Delta P^{+i}_{l(k)}$ is defined as a positive value. Note that both $PTDF^{i}_{k,g\to h}$ and $\Delta P^{i}_{g\to h}$ depend on the outage i. For a generator outage i, the topology remains unchanged, but the redispatch availability of generator g is lost. Thus, $\Delta P^{i}_{g\to h}$ might be different from normal operation since $P^{+i}_{R(g)} = P^{-i}_{R(g)} = 0$. For a line outage i, the redispatch availability remains unchanged, but the topology changes. Thus, we need to recalculate $PTDF^{i}_{k,g\to h}$ for line outages. When we know which generation shift $\Delta P_{g\to h}$ that lead to the largest line flow decrease $\Delta P^{+i}_{l(k)}$, the cost $c^{+i}_{l(k)}$ of the redispatch measure is given by

$$c^{+i}_{l(k)} = (c^{+}_{R,g} + c^{-}_{R,h})\Delta P_{g\to h} \ . \tag{12}$$

With this result, we can calculate $a^{i}_{2(k)}$ and $b^{i}_{2(k)}$ as the affine function connecting (8) and (9).

4) Cascading overload: Short term overloads might be acceptable up to a certain point, but should not be allowed to evolve into cascading events. Here, we consider two types of cascade initiation. First, any overload that cannot be removed by remedial actions might eventually lead to a line trip (delayed trip due to time settings in the relays or flash-over due to sag). We therefore define line loadings higher than $\overline{P}_{l(k)}+\Delta P^{+i}_{l(k)}$ as cascading overload. Second, overloads above a certain threshold (e.g., $P^{i}_{l(k)} > 1.2 \cdot \overline{P}_{l(k)}$) might lead to immediate trip of the line. To avoid this, we introduce a limit for $\Delta P^{+i}_{l(k)}$ (e.g., $\Delta P^{+i}_{l(k)} \leq 0.2 \cdot \overline{P}^{+i}_{l(k)}$).
Since the potential impacts of a cascading event are very high, the severity increases very rapidly as we enter the cascading zone. The increase in severity per additional MW loading is denoted by ρ_C. The severity function parameters $a^{i}_{3(k)}$ and $b^{i}_{3(k)}$ are chosen such that the severity function connects the two points given by (9) and (13). This part of the severity function is marked red in Fig. 1.

$$\boldsymbol{\mathcal{S}}_{(k|i)}(\overline{P}^{i}_{l(k)} + \Delta P^{+i}_{l(k)} + 1) = 1 + a^{i}_{2(k)}\Delta P^{+i}_{l(k)} + \rho_C \tag{13}$$

There are many possible ways of defining the value of ρ_C. On the one hand, if $\overline{\rho}_C \to \infty$, no violation of the limit $\overline{P}^{i}_{l(k)} + \Delta P^{+i}_{l(k)}$ is allowed. On the other hand, if contingency analysis show that an outage of line k following the outage i would not have an adverse effect on the system as a whole, we can choose $\underline{\rho}_C = a_{2(k)}$. The reason for this lower bound is that $\rho_C \geq a_{2(k)}$ to ensure convexity of the severity function (5). Thus, we get that ρ_C can be chosen anywhere in the range $\underline{\rho}_C \leq \rho_C \leq \overline{\rho}_C$. Here, we choose $\rho_C = \max\{120, a_{2(k)}\}$, corresponding to a very rapid increase in the risk as the line loading exceeds $\overline{P}_{l(k)} + \Delta P^{+i}_{l(k)}$. We also assume that ρ_C is the same for all lines, assuming that cascading events should be generally avoided.

C. Risk Constraints

Since the risk is modelled based on the post-contingency line flows , we can formulate risk-based constraints for these line flows. For other quantities, e.g. line flows in normal operation or generator outputs, no risk-based constraints can be formulated, since no risk level is defined for those quantities.

1) Formulation of risk constraints: Based on the risk measures defined by (1) to (4), we can formulate constraints to limit the risk:

$$\boldsymbol{\mathcal{R}}^{spec}: \quad \boldsymbol{\mathcal{P}}_{(i)} \cdot \boldsymbol{\mathcal{S}}_{(k|i)}(P^{i}_{l(k)}) \leq \overline{\boldsymbol{\mathcal{R}}}_{(i)} \tag{14}$$

$$\boldsymbol{\mathcal{R}}^{out}: \quad \sum_{i=1}^{N_{out}} \boldsymbol{\mathcal{P}}_{(i)} \cdot \boldsymbol{\mathcal{S}}_{(k|i)}(P^{i}_{l(k)}) \leq \overline{\boldsymbol{\mathcal{R}}}^{out} \tag{15}$$

$$\boldsymbol{\mathcal{R}}^{line}: \quad \sum_{k=1}^{N_l} \boldsymbol{\mathcal{P}}_{(i)} \cdot \boldsymbol{\mathcal{S}}_{(k|i)}(P^{i}_{l(k)}) \leq \overline{\boldsymbol{\mathcal{R}}}^{line} \tag{16}$$

$$\boldsymbol{\mathcal{R}}^{tot}: \quad \sum_{i=1}^{N_{out}} \sum_{k=1}^{N_l} \boldsymbol{\mathcal{P}}_{(i)} \cdot \boldsymbol{\mathcal{S}}_{(k|i)}(P^{i}_{l(k)}) \leq \overline{\boldsymbol{\mathcal{R}}}^{tot} \tag{17}$$

Eq. (14) constrains the risk for each line k to stay below a constant limit $\overline{\boldsymbol{\mathcal{R}}}_i$ after the outage i. Eq. (15) limits the risk of outage i, while (16) limits the risk of line k and (17) limits the total risk in the system.

2) Relation to N-1 constraints: Including the constraints (14) - (17) in the optimization problem allows us to control the risk level in the system according to our preferences, but also requires us to define the risk limits $\overline{\boldsymbol{\mathcal{R}}}$ in a reasonable way. To provide a physical interpretation of the risk limits, we relate the risk-based constraints (14) to the traditional N-1 constraints. This relation is then used to propose reasonable values for the risk limits, and to show how the choice of the risk limits influences the accepted post-contingency flows.
Assuming that $\boldsymbol{\mathcal{P}}_{(i)}$ is a scalar value given as an input to the optimization, (14) can be reformulated as an upper bound on the severity

$$\boldsymbol{\mathcal{S}}_{(k|i)}(P^{i}_{l(k)}) \leq \frac{\overline{\boldsymbol{\mathcal{R}}}_{(i)}}{\boldsymbol{\mathcal{P}}_{(i)}} \ . \tag{18}$$

If the risk limit is chosen equal to the probability of the outage, $\overline{\boldsymbol{\mathcal{R}}}_{(i)} = \boldsymbol{\mathcal{P}}_{(i)}$, the risk constraint (18) reduces to

$$\boldsymbol{\mathcal{S}}_{(k|i)}(P^{i}_{l(k)}) \leq 1 \ . \tag{19}$$

The severity function, as defined in Section II.B, takes the value $\boldsymbol{\mathcal{S}}_{(k|i)}(\overline{P}^{i}_{l(k)}) = 1$ at the line capacity limit $\overline{P}_{l(k)}$, and $\boldsymbol{\mathcal{S}}_{(k|i)}(\overline{P}^{i}_{l(k)}) \leq 1$ when $P^{i}_{l(k)} \leq \overline{P}_{l(k)}$. Thus, (19) is equivalent to the traditional N-1 constraint $P^{i}_{l(k)} \leq \overline{P}_{l(k)}$.
To enforce the traditional N-1 criterion for the overall system, the upper bound on the severity must be equal to 1 for all risk constraints (14). To achieve this, the risk limit must be set to $\overline{\boldsymbol{\mathcal{R}}}_{(i)} = \boldsymbol{\mathcal{P}}_{(i)}$ for all outages i. This choice implies that the accepted risk level $\overline{\boldsymbol{\mathcal{R}}}_{(i)}$ is different for outages with different outage probabilities $\boldsymbol{\mathcal{P}}_{(i)}$.
This discussion highlights two important characteristics of the traditional N-1 criterion. First, the N-1 criterion corresponds to an implicit risk level, which might be different from the desired risk level. Second, the N-1 criterion leads to a situation where the accepted risk level differs between outages, and is thus inconsistent across the system, because the outage probabilities are not accounted for. These problems of the N-1 criterion can be mitigated by enforcing risk-based constraints with an appropriately chosen, consistent risk limit. The value of this risk limit should be in the same order of magnitude as the outage probabilities, to obtain a risk level which is not too different from the traditional N-1 situation.

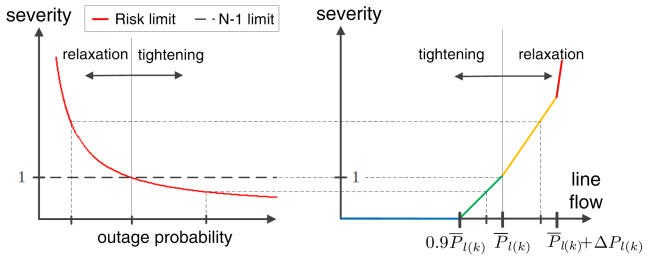

Fig. 2. Left: Comparison between the risk-based severity limit (red line), and the N-1 severity limit (black line). Right: Tightening and relaxation of the line flow constraint as a function of the severity limit and the line and outage specific severity function.

If the risk limit $\overline{\boldsymbol{\mathcal{R}}}_{(i)}$ is chosen to be the same for all outages i, the upper bound on the severity depends on the outage probability $\boldsymbol{\mathcal{P}}_{(i)}$ and a higher severity is accepted for outages with low probability. This is illustrated in Fig. 2 (left), where the red line is the severity limit for a given value of $\overline{\boldsymbol{\mathcal{R}}}_{(i)}$ and the black dashed line is the severity limit for the N-1 criterion (which is constant equal to 1, independent of the outage probability). Since the severity is a function of the post-contingency line flow, accepting a higher (or lower) severity relaxes (or tightens) the constraint on the post-contingency line flow. The amount of relaxation (or tightening) depends on the severity function, as shown in Fig. 2 (right).

III. Formulation of Optimization Problem

This section introduces the risk-based, probabilistic security constrained optimal power flow (RB-pSCOPF), with risk-based constraints for the post-contingency line flows and chance constraints to account for the forecast uncertainty. The objective is to find the minimal cost dispatch that satisfies the desired risk level for all N_{out} outages as well as the desired violation level for the chance constraint. The setup is similar to the probabilistic SCOPF described in [9], but the security constraints for the post-contingency line flows are substituted with the proposed risk-based constraints. In addition to the N_G generators and N_l lines, there are N_B buses, N_L loads and N_w wind power plants in the system. Given a DC power flow formulation, the line flows can be expressed as linear functions of the active power injections both in normal and outage conditions:

$$P_l^i = A^i P_{inj}^i, \quad \text{for all } i = 0, ..., N_{out} \ . \tag{20}$$

Here, $A^i \in \mathbb{R}^{N_l \times N_B}$ describes the relation between the active power injections $P_{inj}^i \in \mathbb{R}^{N_B}$ and the line flows P_l^i after outage i, with $i = 0$ being the normal operation condition. A^i is given by

$$A^i = B_f^i \begin{bmatrix} (\widetilde{B}_{bus}^i)^{-1} & \mathbf{0} \\ \mathbf{0} & 0 \end{bmatrix} \tag{21}$$

where $B_f^i \in \mathbb{R}^{N_l \times N_B}$ is the line susceptance matrix and $\widetilde{B}_{bus}^i \in \mathbb{R}^{N_B-1 \times N_B-1}$ the bus susceptance matrix (without the last column and row) after outage i [9]. The power injections are given by

$$P_{inj}^i = C_G^i(P_G - d^i P_m^i) + C_w^i P_w - C_L^i P_L, \ i = 0, ..., N_{out} \ . \tag{22}$$

$P_G \in \mathbb{R}^{N_G}$ describe the generator output, and $P_L \in \mathbb{R}^{N_L}$ the load consumptions. $P_w \in \mathbb{R}^{N_w}$ contains the wind power infeeds, and is the sum of the forecast P_w^f and a random error ΔP_w. The matrices $C_G \in \mathbb{R}^{N_B \times N_G}$, $C_w \in \mathbb{R}^{N_B \times N_w}$ and $C_L \in \mathbb{R}^{N_B \times N_L}$ relate the power injections to the respective buses. The distribution vector d^i describes how the power mismatch $P_m^i \in \mathbb{R}$ is compensated by the different generators. P_m^i describes the power required to balance wind power deviations and power outages, and is defined as

$$P_m^i = \mathbf{1}_{1 \times N_w}(P_w - P_w^f) - (b_G^i)^T P_G + (b_L^i)^T P_L^f \tag{23}$$

where the first term is the sum of the forecast deviations, and the two next terms corresponds to generator or load outages. $b_G^i \in \mathbb{R}^{N_G}$ and $b_L^i \in \mathbb{R}^{N_L}$ are binary vectors whose elements are either '0' or '1'. A value of '1' corresponds to the tripped component for outage i. The resulting optimization problem is given by

$$\min_{P_G} c_1^T P_G + P_G^T [c_2] P_G \tag{24}$$

subject to

$$\mathbf{1}_{1 \times N_b}(C_G P_G + C_w P_w^f - C_L P_L) = 0 \tag{25}$$

$$\mathbb{P}\left(\begin{array}{c} -\overline{P}_l \le A^0 P_{inj}^0 \le \overline{P}_l \\ \underline{P}_G \le P_G - d^i P_m^i \le \overline{P}_G \ , \quad i = 0, ..., N_{out} \\ \boldsymbol{\mathcal{R}} \ \le \ \overline{\boldsymbol{\mathcal{R}}} \end{array} \right) \ge 1 - \varepsilon \tag{26}$$

Eq. (24) and (25) define the objective function and the power balance constraints, with $c_1, \ c_2 \in \mathbb{R}^{N_G}$ being the linear and quadratic cost coefficients, and $[c_2]$ a diagonal matrix with c_2 on the diagonal. Eq. (26) describes a probabilistic constraint, stating that all inequalities within the brackets must hold with a probability of at least $1-\varepsilon$, where ε is called the violation level. The first inequality is the line flow limits for normal operating conditions $i = 0$, and the second inequality the capacity limits of the generators P_G in all conditions i. The last inequality describes one or more risk limitations for the post-contingency line flows, which can be chosen from the options proposed in Section II.C. The problem remains convex after introduction of the risk constraints. Inserting (22) and (20) in (5), $\boldsymbol{\mathcal{S}}_{(k|i)}(P_{l(k)}^i)$ can be expressed as a the pointwise maximum over a set of affine functions with P_G as an argument. $\boldsymbol{\mathcal{P}}_{(i)} \cdot \boldsymbol{\mathcal{S}}_{(k|i)}(P_{l(k)}^i)$ is hence convex with respect to P_G. This means that all the risk measures are sums of convex functions and hence convex themselves.

A. Chance Constraint Reformulation

In this paper, we follow the probabilistically robust approach, a randomized optimization technique proposed in [11]. This method allows us to account for a reduced number of scenarios inside the optimization compared with the scenario approach [12], while still guaranteeing a violation level $\le \varepsilon$. The method includes two steps. In the first step, we solve an optimization problem to determine, with a confidence of at least $1 - \beta$, the minimum volume set D that contains at least $1-\varepsilon$ probability mass of the distribution of the uncertain variable P_w. The number of required scenarios for this first step is related to the number of uncertain variables N_w and given by [12]

$$N \ge \frac{1}{\varepsilon} \frac{e}{e-1} \left(\ln \frac{1}{\beta} + 2N_w - 1 \right) \ , \tag{27}$$

where e is the base of the natural logarithm. Further details on how to compute D is given in [11], [16]. In the second step, we use the probabilistically computed set D to solve a robust problem for all uncertainty realizations within this set. The chance constraint (26) is substituted by the robust constraints

$$\begin{aligned} -\overline{P}_l \leq A^0 P^0_{inj} \leq \overline{P}_l \qquad & \forall P_w \in D \\ \underline{P}_G \leq P_G - d^i P^i_m \leq \overline{P}_G \ , \ i = 1, ..., N_{out} \ , \qquad & \forall P_w \in D \\ \boldsymbol{\mathcal{R}} \ \leq \ \overline{\boldsymbol{\mathcal{R}}} \qquad & \forall P_w \in D \end{aligned}$$

Since all our constraints are convex with respect to P_w (independent of the value of P_G), the robust constraints hold for all $P_w \in D$ if they hold for P_w at the vertices of the set, i.e., all possible combinations of minimum and maximum values of the vector P_w. With one wind power plant, we need to consider only 2 scenarios, the maximum and minimum P_w in D. With N_w uncertain in-feeds, we must consider 2^{N_w} scenarios. In this case, enumeration of the vertices should be avoided to solve the problem more efficiently. This can be achieved by applying techniques proposed in [17].

B. Possible SCOPF formulations

The risk-based, probabilistic OPF (RB-pSCOPF), given by (24) - (26) includes risk-based limits for the post-contingency line flows and accounts for wind in-feed uncertainty. However, some small changes allow us to change the OPF type. By choosing $\overline{\boldsymbol{\mathcal{R}}}_{(i)} = \boldsymbol{\mathcal{P}}_{(i)}$ for each outage i and $\overline{\boldsymbol{\mathcal{R}}}^{out} = \overline{\boldsymbol{\mathcal{R}}}^{line} = \overline{\boldsymbol{\mathcal{R}}}^{tot} = \infty$, the risk-based constraints become equivalent to traditional N-1 constraints. If the forecast is perfect, i.e. there exist no forecast uncertainty, we set $P_w = P^f_w$ such that the probabilistic constraint (26) reduces to a deterministic constraint. Thus, we can define four different SCOPF formulations:

1) *Standard SCOPF* (SCOPF) considers traditional N-1 constraints (i.e., choose $\overline{\boldsymbol{\mathcal{R}}}_{(i)} = \boldsymbol{\mathcal{P}}_{(i)}$), and no forecast errors for the wind in-feed ($P_w = P^f_w$).

2) *Probabilistic SCOPF* (pSCOPF) considers traditional N-1 constraints (i.e., choose $\overline{\boldsymbol{\mathcal{R}}}_{(i)} = \boldsymbol{\mathcal{P}}_{(i)}$), and a probabilistic constraint with violation level ε.

3) *Risk-based SCOPF* (RB-SCOPF) considers risk-based post-contingency line flow constraints, but no forecast errors for the wind in-feed ($P_w = P^f_w$).

4) *Risk-based, probabilistic SCOPF* (RB-pSCOPF) considers risk-based post-contingency line flow constraints, and a probabilistic constraint with violation level ε.

In the following case study, we compare these four formulations.

IV. Case study

The OPF formulations presented above are applied to the IEEE 30-bus network [18], which is modified to include two wind power generators (i.e., $N_w = 2$) at bus 7 and 12. The forecasted wind power at the two buses is 50 and 40 MW, respectively. To generate wind power scenarios, we used a Markov Chain based model as described in [19], [9]. For the chance constrained optimization, we account for up to 2000 scenarios (depending on ε). In addition, we have 8000 scenarios which are used only for evaluation of the risk. The line outage probabilities were estimated based on the line length (estimated from the line reactance) and the average outage probability for transmission lines in Germany [13]. The generator outages were estimated based on reliability data from the IEEE RTS-96 system [20]. We assume that all generators are able to provide both positive and negative redispatch and that the up and down redispatch capability are the same, i.e., $P^+_R = P^-_R = P_R$. The redispatch capability is defined as 10% of the maximum output for each generator, $P_R = 0.1 \cdot \overline{P}_G$, and all generators are paid the same price for redispatch [$/MW], with $c^+_{R(g)} = 1.1 \max(c_1)$ and $c^-_{R(g)} = 0$. Further, we introduce a new base quantity $\boldsymbol{\mathcal{R}}^{base}$. This quantity is defined as the median probability of the line outages,

$$\boldsymbol{\mathcal{R}}^{base} = \text{median}(\boldsymbol{\mathcal{P}}_{(k)}) \ ,$$

where k denotes the set of all line outages. When we define risk limits $\overline{\boldsymbol{\mathcal{R}}}_{(i)}$ and $\overline{\boldsymbol{\mathcal{R}}}^{out}$ or evaluate the risks $\boldsymbol{\mathcal{R}}^{spec}_{(i,k)}$ and $\boldsymbol{\mathcal{R}}^{tot}$ in the case study, we normalize the values by $\boldsymbol{\mathcal{R}}^{base}$ to obtain numerical values that are easier to interpret. All optimization problems were solved using CPLEX via the MATLAB interface TOMLAB.

A. Generation cost and risk level for different SCOPF formulations

We first compare the generation cost obtained with the four SCOPF formulations presented in Section III.B. The contingency and line specific risk constraint $\boldsymbol{\mathcal{R}}^{spec}_{(i,k)} \leq \overline{\boldsymbol{\mathcal{R}}}$ is used for the risk-based formulations, with $\overline{\boldsymbol{\mathcal{R}}} = \boldsymbol{\mathcal{R}}^{base}$. For the probabilistic formulations, the maximum violation level was set to $\varepsilon \leq 0.05$.

Table I lists the generation cost for each of the four SCOPF formulations. The variation in generation cost is not very large. However, using the risk-based criterion in this case reduces the cost by about 0.1% (RB-SCOPF compared to SCOPF), whereas accounting for wind uncertainty increases cost by about 0.5% (RB-pSCOPF compared to RB-SCOPF).

TABLE I. SCOPF formulations

Formulation	SCOPF	pSCOPF	RB-SCOPF	RB-pSCOPF
Generation cost (% of SCOPF)	100.00	100.48	99.88	100.35

To explain the differences in cost, we compare the risk level for the different formulations. Considering the solutions of the optimization problems above, we compute $\boldsymbol{\mathcal{R}}^{spec}_{(i,k)}$ according to (1). We first discuss the SCOPF and RB-SCOPF solutions, and then move on to the RB-pSCOPF result. Since the SCOPF and RB-SCOPF are deterministic, we compute $\boldsymbol{\mathcal{R}}^{spec}_{(i,k)}$ for the case where no wind deviation occurs, $P_w = P^f_w$. In Fig. 3, the severity $\boldsymbol{\mathcal{S}}_{(k|i)}$ is plotted against $\boldsymbol{\mathcal{P}}_{(i)}$ for each line k and each outage i. The black diamonds and the blue dots are the results from the SCOPF and the RB-SCOPF, respectively. Note that since we calculate the severity for all lines after each outage, there are several dots and circles for each outage. The red line is the risk limit $\overline{\boldsymbol{\mathcal{R}}}_{(i)} = \boldsymbol{\mathcal{R}}^{base}$, and dashed black line is the N-1 limit $\boldsymbol{\mathcal{S}}_{(k|i)} = 1$. For most outages, $\boldsymbol{\mathcal{S}}_{(k|i)} = 0$ for all lines k because all post-contingency line flows are below $0.9\overline{P}_{l(k)}$. For other outages, $\boldsymbol{\mathcal{S}}_{(k|i)} > 0$, but is similar for both the RB-SCOPF and the SCOPF. However, the RB-SCOPF violates the N-1 limit for two cases (i.e., there are two outages with

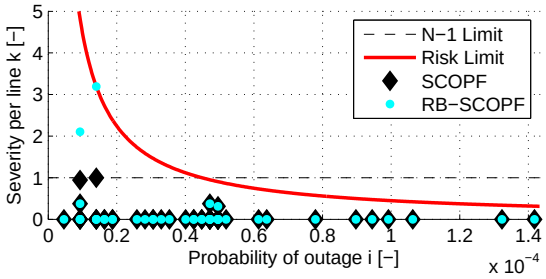

Fig. 3. Comparison of solutions obtained with the traditional SCOPF and the RB-SCOPF. The black diamonds (SCOPF) and the blue dots (RB-SCOPF) show the evaluation of $\boldsymbol{\mathcal{R}}_{(i,k)}^{spec}$ for the case where $P_w = P_w^f$.

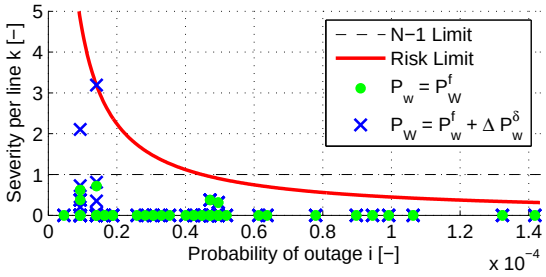

Fig. 4. Evaluation of $\boldsymbol{\mathcal{R}}_{(i,k)}^{spec}$ for the solution obtained with the RB-pSCOPF. The green dots is $\boldsymbol{\mathcal{R}}_{(i,k)}^{spec}$ evaluated for $P_w = P_w^f$. The blue crosses are $\boldsymbol{\mathcal{R}}_{(i,k)}^{spec}$ for the worst-case scenarios $P_w = P_w^f + \Delta P_w^\delta$.

$\boldsymbol{\mathcal{S}}_{(k|i)} > 1$). For one of the binding constraints, the severity is allowed to increase from $\boldsymbol{\mathcal{S}}_{(k|i)} = 1$ with the SCOPF to $\boldsymbol{\mathcal{S}}_{(k|i)} = 3.2$ with the RB-SCOPF. Because of the relaxation of this binding constraint, the cost is lower for the RB-SCOPF than the SCOPF in this case. Note that in other cases, the RB-SCOPF could lead to a more expensive solution than the SCOPF, since the RB-SCOPF leads to a constraint tightening for outages with high probability.

The above discussion for the results of the SCOPF and the RB-SCOPF only considers the risk level for the forecasted wind $P_w = P_w^f$. Looking at the results for RB-pSCOPF, we now discuss how the risk level changes when we account for forecast uncertainty in the optimization. We compute $\boldsymbol{\mathcal{R}}_{(i,k)}^{spec}$ for the case where no wind deviation occurs, $P_w = P_w^f$, and for the cases $P_w = P_w^f + \Delta P_w^\delta$, where δ denotes the worst case scenarios in the robust set D. Fig. 4 shows the risk computed for the solution of the RB-pSCOPF for different wind in-feed scenarios. The green dots show the risk for the wind energy forecast $P_w = P_w^f$, while the blue crosses denote the risk for the worst case scenarios $P_w = P_w^f + \Delta P_w^\delta$. Comparing Fig. 4 to Fig. 3, we see that the RB-pSCOPF leads to lower severities $\boldsymbol{\mathcal{S}}_{(k|i)}$ than the RB-SCOPF when $P_w = P_w^f$ (the green RB-pSCOPF dots are lower than the blue dots of the RB-SCOPF). However, for the worst-case scenario $P_w = P_w^f + \Delta P_w^\delta$, the risk is at the limit (one cross at the red line). By keeping a margin and being conservative for the case with $P_w = P_w^f$, the RB-pSCOPF avoids constraint violations for all $P_w \in D$. This conservativeness affects the generation cost, meaning that the RB-pSCOPF will always be more expensive than the RB-SCOPF.

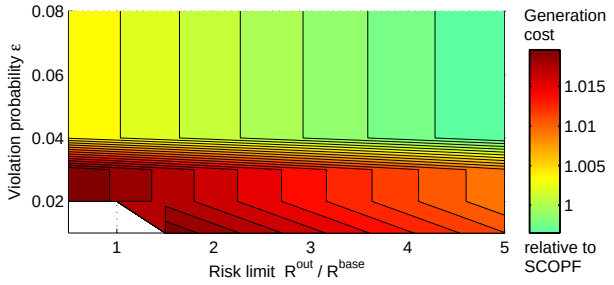

Fig. 5. Generation cost obtained with the RB-pSCOPF, relative to the cost of the SCOPF, for different limits on the violation level ε and the risk $\boldsymbol{\mathcal{R}}_{(i)}^{out} \leq \overline{\boldsymbol{\mathcal{R}}}^{out}$. In the white region, there is no feasible solution to the problem.

Note that in this case, all $\boldsymbol{\mathcal{S}}_{(k|i)} < 1$ for the RB-pSCOPF when $P_w = P_w^f$. This explains why the RB-pSCOPF is more expensive than the SCOPF. This result is however case dependent, and could change with, e.g., a different violation level ε.

B. Influence of risk limit and accepted violation probability on the RB-pSCOPF

We now compare generation cost and risk level for the RB-pSCOPF for different upper bounds on the risk and violation probability. The accepted violation level ε is varied in the range between 0.01 - 0.08. The scenarios are first drawn for $\varepsilon = 0.08$, and additional samples are added as ε is decreased. The upper bound in the contingency specific risk constraint $\boldsymbol{\mathcal{R}}_{(i)}^{out} \leq \overline{\boldsymbol{\mathcal{R}}}^{out}$ is varied in the range $(0.5 - 5)\ \boldsymbol{\mathcal{R}}^{base}$. The generation cost is obtained directly as an output from the optimization, while the risk level $\boldsymbol{\mathcal{R}}^{tot}$ is computed as the average total risk (4) for 8000 wind scenarios.

The generation cost of the RB-pSCOPF for different risk levels $\overline{\boldsymbol{\mathcal{R}}}^{out}$ and violation probabilities ε is depicted in Fig. 5. The cost increases as the acceptable violation level ε or the risk limit $\overline{\boldsymbol{\mathcal{R}}}^{out}$ decreases. This is as expected, since a lower violation probability means that the robust set D becomes larger and a lower risk limit implies shifting the severity curve to lower values. The generation cost is not influenced very much by the choice of ε, except for a cost decrease as ε increases from 0.03 to 0.04. The relaxation of the risk limit $\overline{\boldsymbol{\mathcal{R}}}^{out}$ decreases the cost linearly.

Fig. 6 shows the average total risk $\boldsymbol{\mathcal{R}}^{tot}$ over 8000 wind scenarios. The risk decreases as the acceptable violation level ε or the risk limit $\overline{\boldsymbol{\mathcal{R}}}^{out}$ decreases. The total risk is not very sensitive to the choice of ε, except when ε increases from 0.03 to 0.04. The choice of the risk limit $\overline{\boldsymbol{\mathcal{R}}}^{out}$ has a more significant influence. For $\overline{\boldsymbol{\mathcal{R}}}^{out} < 2.5 \cdot \boldsymbol{\mathcal{R}}^{base}$, the risk increases linearly. For higher risk limits $\overline{\boldsymbol{\mathcal{R}}}^{out} > 2.5 \cdot \boldsymbol{\mathcal{R}}^{base}$, the risk increases quadratically. This means that for $\overline{\boldsymbol{\mathcal{R}}}^{out} > 2.5 \cdot \boldsymbol{\mathcal{R}}^{base}$, the risk level increases faster than the generation cost decreases.

C. Number of cases with overloads

The risk-based formulation allows post-contingency overload (i.e., $\boldsymbol{\mathcal{S}}_{(k|i)} > 1$) for contingencies with low probability. In such cases, post-contingency actions to reduce the line flow are required, which introduce additional cost and require

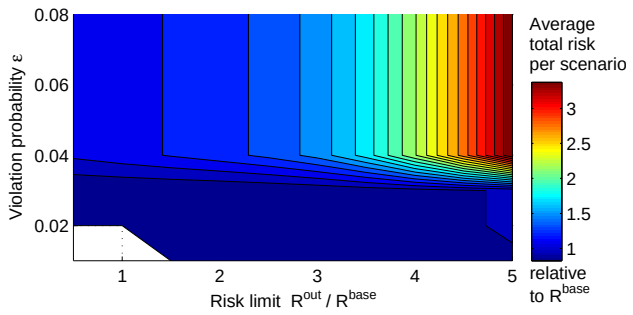

Fig. 6. Average total risk across 8000 wind realizations, normalized by $\boldsymbol{\mathcal{R}}^{base}$. The risk is evaluated for the solutions of the RB-pSCOPF for different limits on the violation level ε and the risk $\boldsymbol{\mathcal{R}}^{out}_{(i)} \leq \overline{\boldsymbol{\mathcal{R}}}^{out}$. In the white region, there is no feasible solution to the problem.

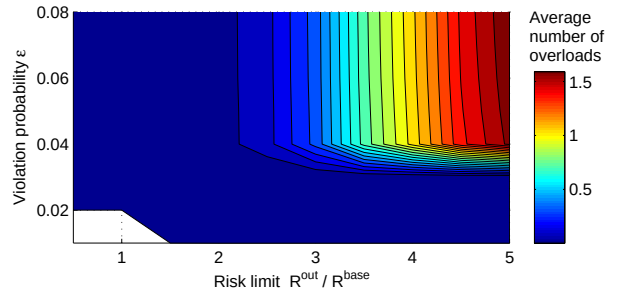

Fig. 7. Average number of N-1 violations across 8000 wind realizations, as obtained with the RB-pSCOPF for different limits on the violation level ε and the risk $\boldsymbol{\mathcal{R}}^{out}_{(i)} \leq \overline{\boldsymbol{\mathcal{R}}}^{out}$. In the white region, there is no feasible solution to the problem.

manual activation by the operator. Since it is not desirable that this happens too often, we investigate how many cases there are with $\boldsymbol{\mathcal{S}}_{(k|i)} > 1$. Investigation A) showed that there were only two outages leading to overloaded lines (i.e., two outages with $\boldsymbol{\mathcal{S}}_{(k|i)} > 1$), even though the risk-based formulations allow post-contingency overloads for all outages with $\boldsymbol{\mathcal{P}}_{(i)} < \boldsymbol{\mathcal{R}}^{base}$. Fig. 7 shows the average number of cases with $\boldsymbol{\mathcal{S}}_{(k|i)} > 1$ for the RB-pSCOPF solutions from the above investigation, evaluated for the 8000 wind in-feed scenarios. Although the number of cases with $\boldsymbol{\mathcal{S}}_{(k|i)} > 1$ increases when either the violation level or the risk limit increases, the average always remains below two violations per scenario. As this is a relatively small number, we believe that these situations can be handled by the operator, particularly since the RB-pSCOPF proposes effective remedial actions to relieve these overloads if the outage should happen.

As an example for the proposed remedial actions, we investigate the redispatch proposed for the RB-pSCOPF case in Fig. 4. The two lines that risk a post-contingency overload (i.e., where the severity is larger than 1) are the lines from bus 6 to 10 and bus 6 to 28. Both would be overloaded if the other is outaged. However, this overload is tolerated since a generation shift of up to 5.5 MW between generator 2 and 4 would be sufficient to remove the overload, with a reduction in the line flow by up to 3.5 MW.

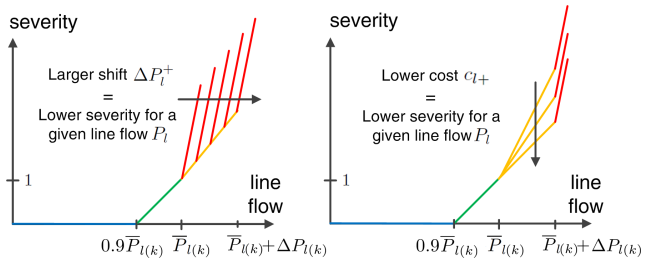

Fig. 8. Left: Change in severity function with higher amount of available redispatch P_R, leading to a higher ΔP_l. Right: Change in severity function with a lower redispatch cost c_+, leading to a less steep severity function.

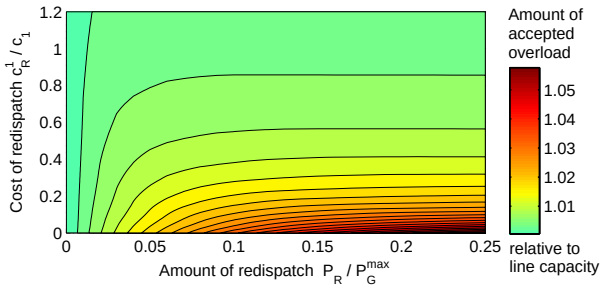

Fig. 9. Average accepted overload for all lines after all contingencies with $\boldsymbol{\mathcal{P}}_{(i)} \geq \text{median}(\boldsymbol{\mathcal{P}}_{(k)})$ (i.e., all contingencies with $\boldsymbol{\mathcal{S}}_{(k|i)} \geq 1$) for different values of P_R and c_R^+. The values are given as a percentage of the line capacity.

D. Influence of cost and availability of remedial measures

If the availability or cost of redispatch change, the severity function changes. Fig. 8 shows the influence of changes in available redispatch power (left) and changes on redispatch cost (right) on the severity function. As more redispatch becomes available or the cost decreases, the severity related to overloads decreases. This means that for some lines, a higher post-contingency line flow will be acceptable. In the following, the influence of the amount and cost of redispatch on the accepted line overloads and objective cost is investigated. The RB-pSCOPF is run with $\varepsilon = 0.05$ and the contingency and line specific risk constraint $\boldsymbol{\mathcal{R}}^{spec}_{(i,k)} \leq \boldsymbol{\mathcal{R}}^{base}$. The amount of available redispatch P_R is varied in the range $(0 - 0.25)\ \overline{P}_G$, and the cost of the redispatch c_R^+ is varied from $(0 - 1.2)\ c_1$ (with $c_R^- = 0$). Fig. 9 shows the average accepted overloads for all lines after all contingencies with $\boldsymbol{\mathcal{P}}_{(i)} \geq \text{median}(\boldsymbol{\mathcal{P}}_{(k)})$ (i.e., all contingencies with $\boldsymbol{\mathcal{S}}_{(k|i)} \geq 1$) for different values of P_R and c_R^+. The values are given as a percentage of the line capacity. If the cost c_R^+ is high, higher amounts of available redispatch P_R does not lead to an significant increase in the accepted overloads. This is because of the steep slope of the severity curve, which means that the accepted overload for most lines is below $\Delta P_{l(k)}$. If the cost c_R+ is low, higher amounts of available redispatch P_R leads to an increase in the accepted overloads. In this case the slope of the severity curve is lower, meaning that the accepted overload is higher than $\Delta P_{l(k)}$. Similarly, if P_R is low, the cost c_R^+ is of little importance, whereas if P_R is high, the accepted overloads are more sensitive to the cost c_R^+.

With more and cheaper remedial actions, it is thus possible to relax the post-contingency line constraints more, which has an influence on the overall cost of the optimization problem.

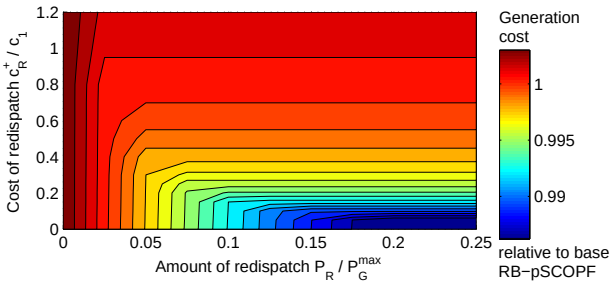

Fig. 10. Cost of the RB-pSCOPF with $\varepsilon = 0.05$ and the contingency and line specific risk constraint $\boldsymbol{\mathcal{R}}_{(i,k)}^{spec} \leq \boldsymbol{\mathcal{R}}^{base}$ for different values of P_R and c_R^+.

Fig. 10 shows the generation cost from the RB-pSCOPF for different values of P_R and c_R^+. The pattern is similar to Fig. 9, confirming that the relaxation of the post-contingency line constraints leads to overall lower cost.

V. Conclusion

This paper proposes a new way of modeling risk in power system operation, accounting for system properties like the effect and availability of redispatch. The resulting risk measure is used to formulate risk-based constraints for the post-contingency line flows. By discussing how the risk-based constraints compares with traditional N-1 constraints, we provide some guidance on how risk limits can be chosen. The new constraints are included in an SCOPF formulation which also accounts for uncertainty of RES in-feeds. This risk-based, probabilistic SCOPF is formulated such that we guarantee that the risk level and the rest of the system constraints will be enforced with a violation level lower than ε, where ε is a design parameter.

The OPF formulation was applied to a case study of the IEEE 30 bus system. We show that we are able to control the risk even when the in-feeds deviate from the forecast. Further, the risk-based formulation allows us to choose the desired risk level, as opposed to the N-1 criterion which only deems the system as secure or insecure. As expected, enforcing a lower level of risk or a lower violation level both increases generation cost, but leads to lower average risk and fewer N-1 violations. The proposed method allows us not only to control the system risk level, but also to account for the effect of available remedial measures during the operational planning process. Through the use of risk-based constraints, the post-contingency line flow limits are set based on which measures are available. The case study demonstrates how the cost and amount of available redispatch influences the severity function, and how less costly and larger amounts of redispatch allow us to relax the post-contingency line flow constraints, leading to lower generation cost.

The method and particularly the severity model can be further developed. Here, the amount of available redispatch is assumed to be known, which allows us to pre-compute the severity function before the optimization starts. In future work, we intend to make the severity function computation part of the optimization, which will allow for co-optimization of the generation dispatch and available redispatch. Further, we would like to include more than one remedial action for each line, and consider the possibility of incorporating other remedial actions than redispatch, such as, e.g., switching actions. Finally, we would like to consider the influence of the remedial actions not only on the overloaded line, but also on other lines in the system.

Acknowledgment

Line Roald receives funding from the project Innovative tools for future coordinated and stable operation of the pan-European electricity transmission system (UMBRELLA), supported under the 7th Framework Programme of the European Union, grant agreement 282775. The research of F. Oldewurtel receives funding from the European Union Seventh Framework Programme FP7-PEOPLE-2011-IOF under grant agreement number 302255, Marie Curie project Stochastic Model Predictive Control, Energy Efficient Building Control, Smart Grid.

References

[1] D. S. Kirschen and D. Jayaweera, "Comparison of risk-based and deterministic security assessments," *IET Gener. Transm. Distrib.*, vol. 1, no. 4, pp. 527–533, 2007.

[2] K. Uhlen, G. H. Kjølle, G. Løvås, and O. Breidablik, "A Probabilistic Security Criterion for Determination of Power Transfer Limits in a Deregulated Environment," in *Cigre Session*, Paris, France, 2000.

[3] F. Xiao and J. McCalley, "Power system assessment and control in a multi-objective framework," *IEEE Trans. Power Systems*, vol. 24, pp. 78–85, 2009.

[4] Q. Wang and J. D. McCalley, "A computational strategy to solve preventive risk-based security constrained OPF," *IEEE Trans. Power Systems*, 2012.

[5] G. Hug, "Generation Cost and System Risk Trade-Off with Corrective Power Flow Control," in *Allerton*, Illinois, USA, 2012.

[6] W. Fu and J. D. McCalley, "Risk-based optimal power flow," in *IEEE PowerTech Conference*, Porto, Portugal, 2001.

[7] L. Roald, M. Vrakopoulou, F. Oldewurtel, and G. Andersson, "Risk-constrained optimal power flow with probabilistic guarantees," in *PSCC*, Wroclaw, Poland, 2014.

[8] Q. Wang *et al.*, "Risk-based locational marginal pricing and congestion management," *IEEE Trans. Power Systems*, vol. 29, no. 5, pp. 2518–2528, 2014.

[9] M. Vrakopoulou, K. Margellos, J. Lygeros, and G. Andersson, "Probabilistic guarantees for the N-1 security of systems with wind power generation," in *PMAPS 2012*, Istanbul, Turkey, 2012.

[10] M. Vrakopoulou *et al.*, "A unified analysis of security-constrained OPF formulations considering uncertainty, risk, and controllability in single and multi-area systems," in *IREP Symposium*, Rethymnon, Greece, 2013.

[11] K. Margellos, P. Goulart, and J. Lygeros, "On the road between robust optimization and the scenario approach for chance constrained optimization problems," *IEEE Trans. Automatic Control*, vol. 59, no. 8, pp. 2258–2263, Aug 2014.

[12] G. Calafiore and M. C. Campi, "The scenario approach to robust control design," *IEEE Trans. Automatic Control*, vol. 51, pp. 742–753, 2006.

[13] M. Obergünner *et al.*, "Using the VDN Statistic on Incidents to Derive Component Reliability Data for Probabilistic Reliability Analyses," *http://www.fgh.rwth-aachen.de/verein/publikat/veroeff /Zuverlaessigkeitskenndaten_gesamt _1994_2001.pdf*, 2004.

[14] F. Xiao *et al.*, "Contingency Probability Estimation Using Weather and Geographical Data for On-Line Security Assessment," in *PMAPS*, Stockholm, Sweden, 2006.

[15] R. Christie, B. F. Wollenberg, and I. Wangensteen, "Transmission management in the deregulated environment," *Proceedings of the IEEE*, vol. 88, no. 2, pp. 170–195, Feb. 2000.

[16] M. Vrakopoulou, K. Margellos, J. Lygeros, and G. Andersson, "A probabilistic framework for reserve scheduling and n-1 security assessment of systems with high wind power penetration," *IEEE Trans. Power Systems*, vol. 28, no. 4, pp. 3885–3896, 2013.

[17] D. Bertsimas and M. Sim, "Tractable Approximations to Robust Conic Optimization Problems," *Mathematical Programming, Series B*, vol. 107, pp. 5–36, 2006.

[18] R. D. Zimmermann, C. E. Murillo-Sanchez, and R. J. Thomas, "Matpower: Steady-state operations, planning, and analysis tools for power systems research and education," *IEEE Trans. Power Systems*, vol. 23, no. 1, pp. 12–19, 2011.

[19] G. Papaefthymiou and B. Klöckl, "MCMC for Wind Power Simulation," *IEEE Trans. Energy Conversion*, vol. 23, no. 1, pp. 234–240, 2008.

[20] C. Grigg *et al.*, "The IEEE Reliability Test System-1996. A report prepared by the Reliability Test System Task Force of the Application of Probability Methods Subcommittee," *IEEE Trans. Power Systems*, vol. 14, no. 3, pp. 1010–1020, 1999.